EPJ Photovoltaics **13**, 26 (2022)

https://doi.org/10.1051/epjpv/2022023

Available online at:
www.epj-pv.org

REGULAR ARTICLE OPEN ACCESS

Exploring reverse-bias characteristics of CIGS solar cells: impact of alkali-post-deposition treatment and CdS buffer layer

Janet Neerken[1], Raymund Schäffler[2], and Stephan J. Heise[1,*]

[1] Ultrafast Nanoscale Dynamics, Institute of Physics, University of Oldenburg, 26111 Oldenburg, Germany
[2] NICE Solar Energy GmbH, Alfred-Leikam-Str. 25, 74523 Schwäbisch Hall, Germany

Received: 14 July 2022 / Received in final form: 10 October 2022 / Accepted: 20 October 2022

Abstract. The characteristics of solar cells in the reverse voltage direction are essential for the resilience of a photovoltaic module against partial-shading induced damage. Therefore, it is important to establish a thorough understanding of the mechanisms that lead to reverse breakdown in solar cells. This work studies thin-film solar cells based on $Cu(In,Ga)Se_2$ (CIGS) absorber layers. Systematic material variations are investigated in order to learn more about the mechanisms governing reverse breakdown in these devices. To this end, devices with different thicknesses of the CdS buffer layer and with and without a RbF-post-deposition treatment (PDT) of the absorber layer were fabricated. The resulting current-voltage characteristics at negative voltage biases reveal that devices break down at much more negative voltages if they underwent a PDT, if the buffer layer thickness is increased, or if the buffer layer is not photoexcited. This implies that possibly a PDT may be disadvantageous for the shading tolerance of a module. The further analysis indicates that several mechanisms are involved in the reverse breakdown. Whereas tunneling currents in the buffer layer seem to play a major role for the actual breakdown, the strong effect of the PDT is probably caused by a reduction of shunt leakage currents along grain boundaries which lowers material heating.

Keywords: Reverse breakdown / partial shading / post-deposition treatment / buffer layer / shunt leakage currents

1 Introduction

An ideal diode blocks currents in the reverse direction. In real diodes and solar cells, however, the blocking behaviour breaks down at sufficiently high negative voltages. Upon breakdown, usually an appreciative amount of electric power is dissipated in the diode which increases the temperature and can lead to permanent damage [1,2]. This can become a problem for photovoltaic solar modules when they are partially shaded: Since in a module the individual cells are commonly connected in series, all cells across a module operate at the same current and their voltages add up. As a consequence, if one cell is shaded, the cumulated photovoltage of the non-shaded cells is applied to the shaded cell in the reverse direction, which may exceed the blocking capabilities of that cell and force it into breakdown. In such a situation, the shaded cell will operate at the photocurrent of the illuminated cells. Hence, the more negative the voltage at which the blocking behaviour starts to break down, the higher the dissipated power in the shaded cell and the more likely it is that it will be irreversibly damaged. On the other hand, cells with a reversible low-voltage breakdown may act as an internal bypass. Therefore, a profound understanding of the mechanisms of reverse breakdown and their link to material parameters is necessary for the production of high-quality industrial modules, in order to be able to tune the breakdown and ensure its reversibility.

In thin-film solar cells that are based on chalcopyrite $Cu(In,Ga)Se_2$ (CIGS) absorber layers several mechanisms have been discussed to drive reverse breakdown [3]. Since the observed negative temperature coefficient of the breakdown voltage is not in line with avalanche breakdown via impact ionization [4,5], it is believed that the reverse breakdown is driven by tunneling processes in CIGS solar cells. Towards negative voltages the bending of the energy bands increases, so that their spatial distance gets smaller and the probability for electrons tunneling from the valence to the conduction band is increased. However, measured breakdown voltages in CIGS are unlikely to be explained by direct band-to-band tunneling [6]. Instead, breakdown has been proposed to take place at the absorber/buffer interface over a triangular potential barrier (Fowler–Nordheim theory) [7] and/or via defect levels in the band gap (e.g. Poole–Frenkel theory) [6].

* e-mail: Stephan.Heise@uni-oldenburg.de

Besides the actual origins of reverse breakdown currents, breakdown in CIGS devices has been shown to occur in very localised areas [8] due to lateral material inhomogeneities [9]. At these "hot-spots" reverse currents induce Joule-heating of the surrounding material [10]. Since tunneling currents and also ohmic shunt leakage currents are sensitive to temperature, an increase in temperature gives rise to a further increase of the currents. In this way, a negative-feedback loop can be established which leads to thermal runaway and may cause permanent damage as mentioned above.

In this study we investigate the reverse breakdown behaviour of CIGS solar cells depending on whether their absorber layers were treated with RbF or not. Such a post-deposition treatment (PDT) with alkali elements has become very common over the past decade because it can improve cell efficiencies [11,12]. The main reason for the performance gain seems to be an increase in open-circuit voltage (V_{OC}) [13], but also the short-circuit current density (J_{SC}) benefits from the possibility to reduce the thickness of the CdS buffer layer [14]. However, despite the popularity of the alkali-PDT, its impact on the reverse breakdown has not been examined yet to the best of our knowledge.

The goal of the study is twofold: On the one hand, we intend to show how a RbF-PDT and a thinning of the CdS buffer layer may affect the reverse breakdown characteristics in order to estimate the consequences of the technology on the shading tolerance of corresponding modules. On the other hand, we utilize the results on the different cell variations in order to learn more about the mechanisms that drive the reverse breakdown in CIGS devices.

2 Methods

2.1 Samples

The samples used in this study were fabricated with the typical layer stack of a ZnO:Al/i-ZnO window layer, a CdS buffer layer and a co-evaporated CIGS absorber layer on a Mo-coated soda-lime glass substrate. For half of the samples a PDT with RbF was applied after the absorber growth. A variation of the buffer layer thickness (20, 30 and 50 nm) was achieved by varying the duration of the chemical bath deposition (CBD). Standard cell efficiencies were in the range of 15%. Details on the photovoltaic parameters are given in Section S.1, which show that the RbF-PDT process already allows for thinner buffer layers and higher J_{SC}, but may be improved regarding V_{OC} and fill factor.

Lab-scale samples were cut from the center of full-size structured modules and reduced to an active area of 0.4 cm^2 by mechanical scribing. Here, illuminated lock-in thermography images (ILIT) ensured that only material without localised hotspots was selected. The cells were contacted outside the active area on the Mo of the active cell (back contact) and the neighbouring cell (front contact via the monolithic series interconnect). For each cell variation, nine individual cells were prepared.

2.2 Experimental techniques

All current–voltage (IV) characteristics were measured in a four-point-probe configuration using a Keithley 2400 source meter. Prior to the measurements the cells were pretreated with 10 min of light soaking under white light of 1000 W/m^2. IV curves were taken at standard test conditions with a PET SS100AAA solar simulator and also in the dark at 25 °C.

The reverse characteristics were determined in the same setup via a voltage sweep from positive to negative voltages (down to −6 V), where the sweeps were done as quickly as feasible (integration time: 20 ms) to minimize potential effects of sample heating. Half of the samples per cell type were measured using a neutral density filter with a transmission of 70% after the AM1.5-like illumination, and the other half were measured using a longpass filter with a cutoff-wavelength of 600 nm (which we will refer to as "red illumination" in the following). In this way the illumination intensities were in a similar range during the reverse measurements.

External quantum efficiencies (EQE) were measured in a Bentham PVE300 system. EQE spectra were obtained without light bias for determining the Urbach energies, and with red light bias when checking for buffer photodoping.

To determine the absorber doping density, capacitance-voltage (CV) measurements were performed in the dark at a frequency of 30 kHz and an AC oscillation level of 30 mV using a Solartron 1260A impedance analyser. For the Mott-Schottky analysis a $C_p - R_p$ equivalent circuit and a dielectric constant of $\varepsilon_{CIGS} = 13.6$ were assumed.

Temperature-dependent IV measurements were performed in a closed cycle helium cryostat (CryoVac). A LakeShore 336 temperature controller was used to apply temperatures in the range from 30 K to 300 K. Illumination was provided by a Xenon lamp with a spectral water filter whose intensity was calibrated such that the short-circuit current of the device under test matched its short-circuit current measured under the calibrated AAA solar simulator of the standard IV setup described above.

Raman spectra were measured on a Bruker Senterra setup in a range of 60 cm^{-1} to 1900 cm^{-1} with a laser excitation of 2 mW at 488 nm and a spot diameter of approximately 1 μm.

2.3 Breakdown voltage

Several suggestions have been brought forward on how to quantitatively determine the voltage at which the blocking behaviour of the diode breaks down from the reverse IV curve [7,15,16]. In this article we are going to use the term "breakdown voltage" in a more qualitative way, because the results and conclusions given here do not depend on the exact definition of the breakdown voltage (this is demonstrated in Sect. S.2). However, we follow the convention to refer to a breakdown voltage as "higher" (or "lower") if it is more (less) negative.

3 Results

The reverse IV characteristics for all fabricated cell variations under white and red illumination are shown in Figure 1. Apparently the cell variations show very clear

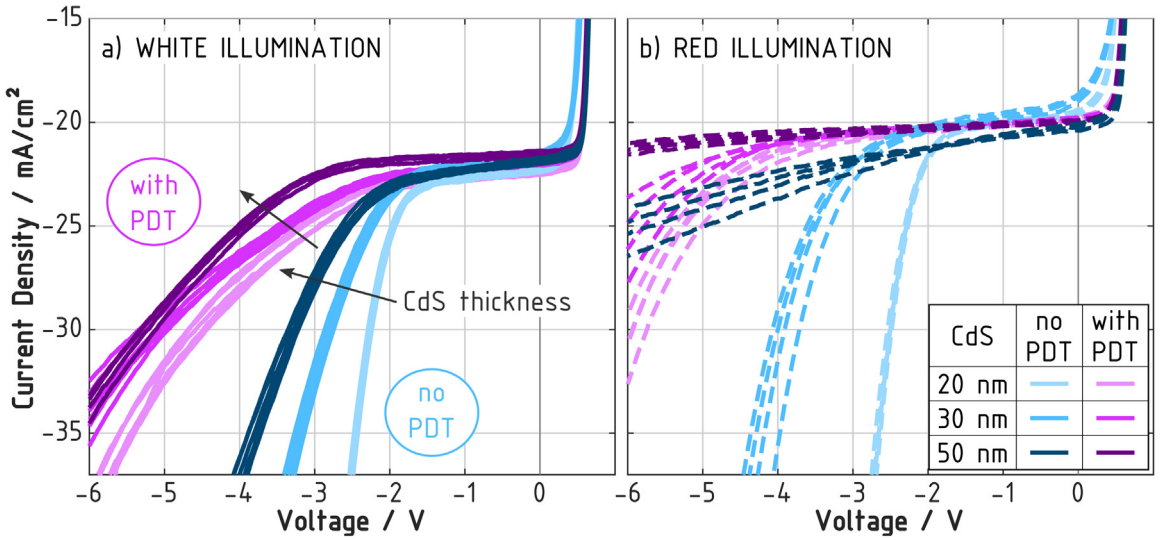

Fig. 1. IV characteristics of samples without PDT (blue) and with PDT (pink) and with different CdS buffer layer thicknesses under (a) white illumination and (b) red illumination (longpass-filtered above 600 nm). Four to six samples per cell type are shown.

differences in their breakdown behaviour, the fluctuations between cells of the same type being much smaller than the differences between cell types or illumination conditions.

Three main results regarding the breakdown behaviour can be read from the IV characteristics in Figure 1:

- The breakdown voltage is significantly higher for cells with a RbF-PDT than for cells without a PDT. This is particularly clear for the case of white illumination, but also holds for red illumination if samples with equal buffer thicknesses are compared. For the situation of a partially shaded module, the higher breakdown voltage of material with PDT implies that also the dissipated power during operation under breakdown is higher, so that the probability of permanent damage upon shading should be increased.
- The breakdown voltage increases with increasing thickness of the CdS buffer layer. This seems to be true regardless of whether samples underwent a PDT or not (although the shapes of the IV curves slightly differ), and it is in line with our previous findings on similar material and buffer thicknesses of 30, 60 and 90 nm [5].
- The breakdown voltage is much higher under red illumination than under white illumination of similar intensity. This effect is somewhat less pronounced in the two cell types without PDT and buffer thicknesses of 20 nm and 30 nm.

In the following, we discuss what may be learned from these results about the mechanisms governing the reverse breakdown by relating our results to findings in literature.

4 Discussion

In a first step, we investigate how property changes of the CdS buffer layer influence the reverse characteristics. The idea is to get a basic picture of the possible mechanisms that could be involved in the reverse behaviour in our samples, before looking at the effects of the alkali-PDT. In a further part, we examine the role of shunt leakage currents for the reverse breakdown.

4.1 Buffer thickness

As a first buffer variation, the thickness of the CdS layer was adjusted to 20, 30 and 50 nm. From Figure 1a it is apparent that the breakdown voltage increases with increasing buffer thickness. This obvious influence of the buffer thickness suggests that tunneling currents inside the buffer layer may play an important role for the reverse breakdown: With decreasing layer thickness the distance between the bands would shrink and the tunneling currents would increase. The tunneling could take place across a triangular potential barrier (Fowler-Nordheim mechanism) or/and via an electronic defect level in the buffer layer (Poole-Frenkel mechanism).

For a quantitative analysis, Szaniawski et al. [7] assumed that the total applied voltage drops inside the buffer layer[1]. Then the electric field E in the buffer layer can be approximated by the applied voltage divided by the buffer thickness, so that the electric field increases with decreasing buffer thickness[2]. In order to check whether the observed IV characteristics can be explained with the Fowler-Nordheim model, a plot of $(J-J_{SC})/E^2$-vs-$1/E$ may be analysed for linearity [7] (where J is the current density). Applying this method to our data reveals that in a range of approximately 1 V above the breakdown voltage

[1] Indications that the buffer layer is fully depleted have been reported [17]. However, the situation would be similar if not the total voltage but only a fixed part of it would drop inside the buffer layer.

[2] A further thickness-dependent influence on the electric field could be caused by Cd-indiffusion into the CIGS layer which makes the absorber less p-type and is assumed to increase with increasing CdS thickness [18].

the IV curves seem to follow the Fowler-Nordheim approach (see Sect. S.3). Similarly, the applicability of the Poole-Frenkel model may be tested by analysing the linearity of a plot of $(J - J_{SC})$-vs-$\sqrt{E}$. Again, our data show a linear dependence for roughly 0.5–1 V above the breakdown voltage.

So it seems that, directly after the onset of breakdown, both discussed tunneling mechanisms are able to explain the dependence of the illuminated reverse breakdown on the thickness of the buffer layer in the investigated samples, which indicates that a mixture of both mechanisms may be at work in this region. At higher negative voltages additional effects seem to set in, possibly due to an increase in temperature. For the Poole-Frenkel mechanism the results imply, that the relevant tunneling defect level would have to be located in the buffer layer, so that the tunneling process is directly affected by the thickness-dependent electric field. In contrast, the model proposed by Sun et al. [6] assumes that the defect level is located in the *absorber* layer in the illuminated case. However, results by Mansfield et al. [19] who observed a non-correlation of absorber thickness and reverse breakdown further support the assumption that the electric field in the absorber layer does not play a big role for reverse breakdown, and that the voltage drop in the buffer layer is more crucial.

Interestingly, the observed increase in breakdown voltage with increasing buffer thickness has also been found in previous studies [4,7,20], but only for the *dark* IV characteristics. This seems to suggest that the relevant mechanisms for reverse breakdown which depend on the buffer thickness are the same in the dark and under illumination. Correspondingly, the data by Szaniawski et al. [7] are also best explained by a mixture of Fowler-Nordheim and Poole-Frenkel tunneling. However, for the reverse breakdown under blue illumination Szaniawski et al. [4,7] did not find such a clear correlation, neither for CdS nor for ZnSnO buffers. A possible explanation could be that in their material the illumination induces photodoping in the buffer layer which makes the layer more *n*-type (e.g. [21]). This would reduce the voltage drop in the buffer layer and increase it in the absorber layer, so that the voltage drop in the buffer layer may be less important for the breakdown characteristics. In our samples we could not detect any evidence for buffer photodoping via red-light-biased quantum-efficiency measurements, so that this effect does not seem to be necessary to consider here.

In conclusion, it seems that in the investigated samples the voltage drop in the buffer layer is critical for the reverse breakdown by influencing the tunneling currents in the buffer layer.

4.2 Buffer excitation

A second variation of the buffer layer properties was achieved by modifying the spectrum of the illumination: Under white (AM1.5) illumination, high-energy photons generate electron-hole pairs inside the CdS layer, whereas this mechanism may be prevented if the illumination is restricted to wavelengths above the CdS band gap ($\lambda_g^{CdS} \approx 500$ nm). The comparison of the reverse IV characteristics under white and red illumination in Figure 1 reveals that most cell types show a significant increase of the breakdown voltage under red illumination, so that they look more like what is known from the reverse behaviour under *dark* conditions (see e.g. [4, 15]). It should be noted here, that we can confirm from previous studies that this large effect is indeed due to the different *spectrum* of the illumination and not caused by the slight differences in *intensity*.

This effect of the illumination spectrum on the reverse breakdown seems to be quite general for chalcopyrite devices, since it has been observed in several other studies [7,15] which also included $CuInS_2$ absorbers [22] and ZnSnO buffers [4]. Judging from the data in Figure 1 it seems that the buffer-thickness dependence of the reverse breakdown is not altered in a significant way by the change of illumination spectrum. Previous studies have also shown that the qualitative temperature dependence of the breakdown is independent of the illumination spectrum [4,15]. This suggests that the fundamental (tunneling) mechanisms of reverse breakdown in CIGS remain unchanged, and only the boundary conditions are modified by the illumination spectrum.

In literature, three different explanations have been brought forward for the spectral effect: First, Braunger et al. [22] suggested that the photoconductivity of the CdS layer, induced by white illumination, increases shunt leakage currents via the CdS layer and thus reduces the breakdown voltage. The influence of shunt leakage currents will be discussed in more detail below (Sect. 4.4). However, judging from the shunt resistances (Fig. S.3), leakage currents do not seem to increase significantly in our samples when the illumination is changed from red to white. Therefore, the buffer photoconductivity is a very unlikely reason for the significant spectral effect we observe.

Secondly, Mack et al. [23,24] suggested that in the case of red illumination, when the CdS buffer is not photoexcited, a pile-up of negative charges may occur at the buffer-absorber interface which is neutralized in the case of "blue" or white illumination by excess holes generated in the buffer layer. This pile-up of negative charges would affect the electric field in the vicinity of the heterointerface and could thus influence tunneling currents in the reverse-bias regime, which is in line with our results. This hypothesis could also explain why the two cell types with 20-nm and 30-nm buffers without PDT are affected much less by the photoexcitation of the buffer: Monitoring the V_{OC} under red illumination over time reveals a decrease of the V_{OC} transients in these two cell types (these measurements were done by colleagues at the Martin Luther University Halle-Wittenberg). This indicates that these cells are limited by interface recombination [25,26] (also seen in the V_{OC}, cf. Tab. S.1), so that charges rather recombine at the interface instead of piling up. Therefore, these breakdown voltages show a much smaller red-light increase when buffer photoexcitation is prevented than in the other cell types.

So while the mechanism of charge pile-up can nicely explain the effect of illumination spectrum on the reverse IV characteristics, it somewhat conflicts with the hypotheses used above to explain the influence of buffer thickness: The pile-up model proposed by Mack et al. [23] implies that

the voltage drops primarily in the CIGS layer under white illumination, and that the voltage drop is constrained mostly to the buffer layer only when interface charges are present under red illumination. However, for explaining the thickness dependence—which is qualitatively preserved under red illumination—we had to assume that the voltage drops primarily in the buffer layer. One possibility to resolve this disagreement would be to assume that a certain amount of interface charges is always present and thus ensures that the voltage drops mainly in the buffer layer, and that the pile up of electrons in the cases of no or red illumination would only add to these interface charges. Whether such a model could quantitatively predict the results of Figure 1 would need to be verified by numeric simulations. Another questionable consequence of the pile-up hypothesis is that it would predict a lower breakdown voltage for thicker buffer layers, since a thicker buffer provides more free holes which could neutralize the pile-up more effectively. Apparently, this disagrees with our experimental results.

Both explanations given above attribute the spectral effect to a consequence of photogeneration inside the buffer layer. However, Szaniawski et al. [4] observed a difference between dark and blue breakdown characteristics even for a narrow-band illumination spectrum at 450 nm which did *not* generate photocarriers in the wide-gap ZnSnO buffer layer. Therefore, they proposed that the spectral effect is caused by the CIGS absorber layer instead: Close to the front interface red and blue illumination could differently modify the charge of static defects—possibly due to a different electron/hole availability—so that the local electric field and thus the breakdown voltage would be changed. Regarding the tunneling mechanism via electronic defect levels as assumed in the Poole-Frenkel model, this illumination-induced change in defects might also lead to a change in tunneling currents via these defects. This would be similar to the model by Sun et al. [6] who suggested that the dominant tunneling channel changes from a deep defect in the CdS layer in the dark to a much shallower defect in the CIGS layer under white illumination. So in combination, this defect-related mechanism is able to explain our experimental findings in Figure 1, if indeed red illumination leads to a reduced electric field in the buffer layer compared to blue illumination. Yet, the origin of these defects and how they relate to a change in breakdown voltage upon light soaking and dark annealing [23] remain to be shown.

4.3 Effects of PDT

The discussion of the buffer influence has shown that the investigated devices seem to exhibit a fairly typical breakdown behaviour in comparison to other CIGS studies. So now that we have developed a basic idea of which mechanisms could play a role for the reverse breakdown in our cells, we next study how a RbF-post-deposition treatment might affect these mechanisms. Figure 1 showed that a RbF-PDT significantly alters the reverse IV characteristics in that the breakdown voltage is increased compared to cells without PDT. Interestingly, the role of the CdS buffer layer seems to be similar in cells with and without PDT, which indicates that the mechanisms of reverse breakdown are not changed completely, but are subjected to certain modifications upon a PDT. In order to analyse the physics behind these modifications, we check a number of effects that an alkali-PDT has been reported to have on CIGS devices and examine how these effects could influence the reverse behaviour of our samples.

4.3.1 Electrostatic potential fluctuations

The reduction of electrostatic potential fluctuations in the absorber layer has been proposed to be the main reason for the improved performance of devices with heavy-alkali-treated absorbers [12,27]. Potential fluctuations could also lead to changes in the reverse IV characteristics, because they will affect the spatial distances between the bands for any tunneling processes involved. So tunneling currents should be reduced if potential fluctuations are decreased by the PDT. This would lead to a higher breakdown voltage in cells with PDT, which is in qualitative agreement to what we observe.

Since potential fluctuations are one of the mechanisms that lead to tail states [12], we analysed the Urbach energy E_U in our samples. Urbach energies were extracted as the inverse slope of a linear fit to the logarithmic EQE as a function of photon energy [28] for three samples per cell type. The results are shown in Figure 2. For all cell types we observe a small, but significant *enlargement* of E_U of about 1.2 meV on average for RbF-treated cells compared to cells without PDT. This indicates that potential fluctuations are not reduced upon PDT in our samples (correspondingly, cells with PDT showed a slightly lower V_{OC} than cells without PDT for 50 nm CdS thickness, see Sect. S.1). Therefore, potential fluctuations in the absorber layer cannot explain the big difference in reverse IV characteristics observed between cells with and without PDT.

4.3.2 Doping density

Commonly, an increase in absorber doping density is observed after an alkali-PDT [29]. In line with these findings, also the samples investigated in the current study show a slight increase in doping upon PDT by a factor of approximately 1.5 (from 1.5 to 2.2×10^{16} cm^{-3} on average) as derived from capacitance-voltage measurements on five samples per cell type. Concerning the tunneling mechanisms, a higher absorber doping should lead to a stronger electric field in the buffer layer, thus facilitating tunneling and *reducing* the breakdown voltage upon PDT. In line with this picture, an inverse relationship between breakdown voltage and doping density has been reported by Puttnins et al. [15] for CIGS devices with a variation of the Na content. The PDT-induced breakdown changes in our samples, however, evidently contrast with this explanation, suggesting that the slight increase in bulk doping density is not responsible for the substantial change in breakdown voltage.

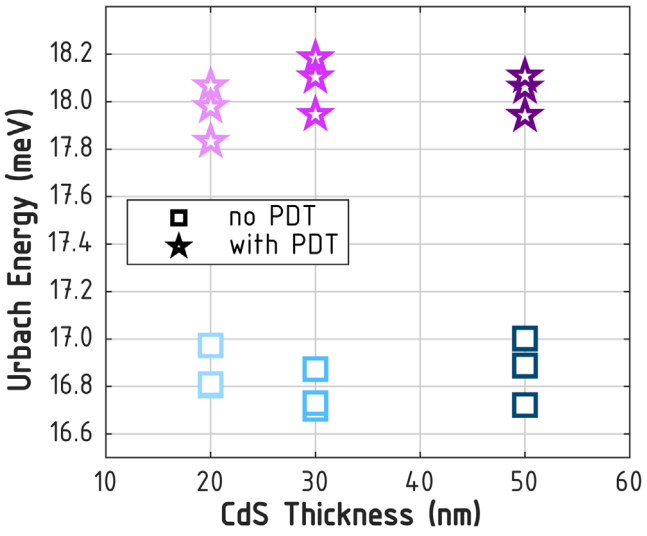

Fig. 2. Urbach energy for the investigated cell types, derived from EQE spectra of three samples per cell type.

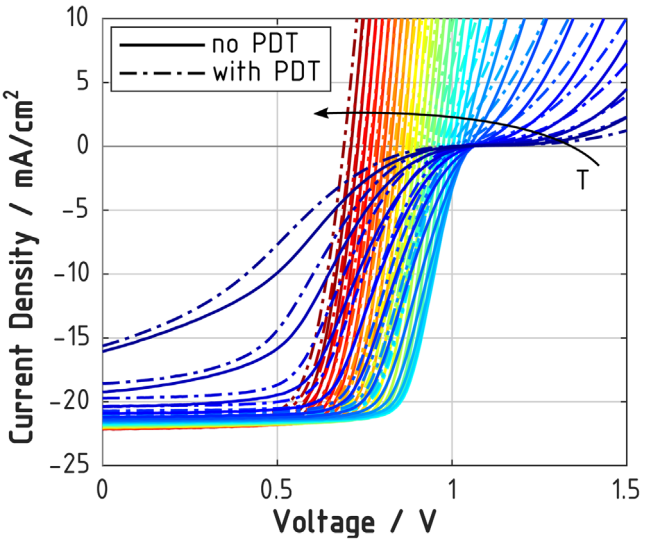

Fig. 3. Temperature-dependent IV characteristics of a sample without PDT (solid line) and with PDT (dashed-dotted line) with a 50-nm thick CdS buffer layer under white illumination of 0.7 kW/m² between 30 K (blue) and 300 K (red).

However, even though the doping density may increase in the CIGS *bulk* upon PDT, indications have been reported that the situation may be different close to the absorber-buffer interface: During the chemical-bath deposition of the CdS buffer layer, Cd atoms tend to occupy Cu vacancies and thus form Cd_{Cu} antisite donors, which make the CIGS absorber more n-type in the vicinity of the interface [30]. This process seems to be facilitated by a KF-PDT [14]. Atom-probe-tomography results suggest that a similar effect can be expected to take place in the case of a RbF-PDT [12]. So if the absorber doping is indeed reduced close to the interface (or likewise the buffer doping [31]), the electric field in the buffer layer may also be reduced and thus the breakdown voltage increased which is in line with the observed behaviour. However, a weaker doping at the interface would effectively also reduce an extraction barrier at the buffer/absorber interface. This hypothesis is probed in the following section.

4.3.3 Interface barrier

Since the alkali-PDT is applied to the bare absorber surface, it is not surprising that it has been shown to affect the buffer/absorber interface: In some devices an alkali-In-Se layer has been detected [32], and a widening of the absorber band gap has been observed at the buffer/absorber interface [33]. If such changes would modify an existing extraction barrier [34]—e.g. a conduction-band spike at the buffer/absorber interface—, this could affect the reverse IV characteristics, because a change in barrier height would change the Fowler-Nordheim tunneling current over that barrier. Indeed, PDT has been found to increase a transport barrier, but this barrier is most likely related to conduction-band offsets at the buffer/window interface and limits the injection and not the extraction of charge carriers [12,35].

In order to analyse whether the PDT modifies any barriers that could affect the reverse breakdown in our samples, we performed temperature-dependent IV measurements. Figure 3 shows the results of a sample with PDT and a sample without PDT (results on a second set of samples were virtually identical). It can be seen that towards low temperatures ($T < 120$ K) an S-shape with decreasing fill factor evolves which indicates an extraction barrier (see e.g. [36]). However, this barrier seems to have almost the same height for the sample with and without PDT. Therefore we conclude, that the large effect of PDT on the reverse breakdown cannot be explained by a change in the height of an extraction barrier.

Figure 3 shows a second barrier in the injection regime (above V_{OC}), which exhibits differences between the sample with and without PDT: IV curves for the sample with PDT start to deviate from the exponential shape at higher temperatures than the IV curves for the sample without PDT. However, it seems unlikely that this barrier could significantly affect the reverse IV characteristics since (i) it limits the *injection* of charge carriers, and (ii) it does not seem to be linked to the buffer layer (see Sect. S.5).

4.3.4 Buffer homogeneity

The results in Sections 4.1 and 4.2 demonstrated that the CdS buffer layer plays an essential role in the reverse breakdown of the investigated devices. Since the quality of the CdS layer has been shown to change upon an alkali-PDT (so that it takes less CBD time to form a high-quality junction) [14], we checked whether differences in the lateral homogeneity of the buffer layer thickness may be present between samples with and without PDT. To this end, we measured Raman spectra on two samples with a 50-nm thick buffer layer at 200 points each. In order to obtain

representative statistics, 20×20 μm^2 maps (25 points each) were recorded at eight regions distributed across the sample area. As an indicator for the buffer thickness we analysed the Raman peak at 300 cm^{-1}, which corresponds to the first order longitudinal optical Raman mode of CdS. Since the penetration depth was larger than the CdS thickness (a CIGS peak was always visible), the height of the CdS peak was used as an indicator of the layer thickness.

Apart from a very similar average peak height, the samples with and without PDT also showed a very comparable homogeneity of the CdS thickness: The coefficients of variation (standard deviations normalized to the mean values) of the peak heights were 4.14% for the sample without PDT and 4.08% for the sample with PDT. Thus, it seems unlikely that the large effect of PDT on the reverse breakdown is caused by an improved homogeneity of the buffer thickness.

To summarize, we found that several of the well-known effects of an alkali-PDT actually do *not* seem to be responsible for the significant increase of the breakdown voltage observed in our devices. As a further mechanism potentially affecting reverse breakdown we next discuss shunt leakage currents.

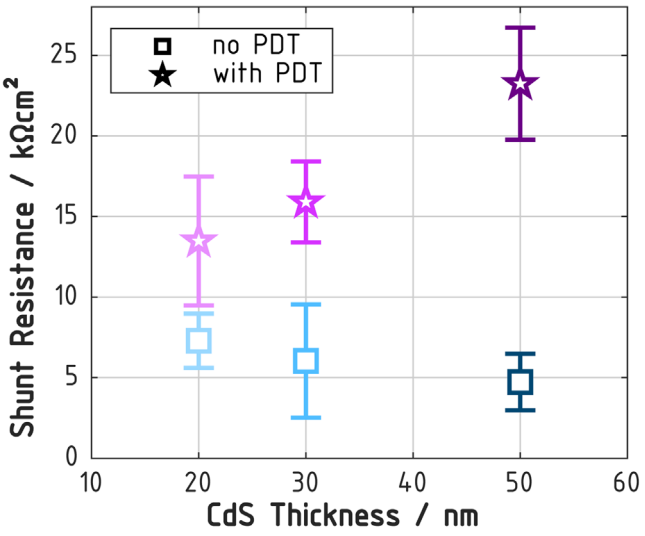

Fig. 4. Shunt resistances of the investigated cell types as extracted from dark IV curves. Mean values (symbols) and standard deviations (error bars) across 8–9 samples per cell type are given.

4.4 Shunt leakage currents

In addition to the tunneling mechanisms described above, the breakdown characteristics may also be affected by shunt leakage currents: Since the amount of leakage currents will control the Joule-heating of the material in the vicinity of the local shunts and since the tunneling mechanisms are very sensitive to temperature, the onset of breakdown can be influenced by the amount of leakage currents indirectly.

Shunt leakage currents across the device may be quantified by the shunt resistance R_{sh}, which is sensitive to changes in both the number or size of local shunts as well as the effectiveness of local shunt paths. In order to analyse possible influences of shunt leakage currents on the reverse breakdown, the shunt resistance was determined as the inverse slope of the dark IV curve at voltages between −0.3 V and 0 V. The results are given in Figure 4.

Regarding the influence of an alkali-PDT on the breakdown characteristics, the results in Figure 4 reveal that the cell types with PDT show a significantly higher R_{sh} than cells without PDT in the current study. This clear difference suggests that the higher shunt resistance may be the key factor behind the higher breakdown voltages in cells with PDT. A higher R_{sh} implies that either PDT leads to more homogeneous material with less (or smaller) shunts, or/and PDT reduces the leakage currents in existing shunts. Both aspects will be discussed in more detail in the following.

First, we look at the nature of the shunt currents in our devices. Several shunt mechanisms have been discussed for CIGS in the literature, which can be distinguished by their voltage dependence of the leakage currents [37]: Whereas pinholes in the absorber layer or shunt paths along grain boundaries give rise to ohmic current-voltage characteristics, space-charge-limited currents (SCLC)—possibly due to imperfections of the buffer/absorber interface [18]—show a power-law IV dependence with an exponent of two or larger, and tunneling mechanisms exhibit an exponential voltage dependence.

As Zelenina et al. [18] pointed out, a simple method to identify the dominating shunt mechanism is to analyse the slope of the IV curve in a double-logarithmic representation, which yields the exponent of a power-law relation. That is, an ohmic shunt should give a slope of one, whereas SCLC should give a slope of two or above. To analyse the nature of the shunt leakage currents in the current study, Figure 5 shows averaged dark-IV curves for all investigated cell types in the range between −1 V and 0 V. The data reveal a very consistent slope for all cell types with a value around one. This indicates that the shunt resistance in our devices is essentially governed by *ohmic* leakage currents. Thus, even though several studies have reported that SCLC influence the shunt resistance in their CIGS solar cells [18,37,38] and Zelenina et al. [18] even observed a reduction of SCLC upon a KF-PDT, SCLC do not seem to play a role in our devices.

One commonly discussed ohmic shunt path in CIGS solar cells is the P1 scribe of the monolithic series interconnects [39]. Since we made use of the interconnects for contacting the samples, any shunt currents across the P1 scribe should contribute to the measured shunt resistances. Shunt currents across the P1 scribe are governed by the resistivity of the absorber material [40], which may be altered by the absorber doping density. However, since the doping is only changed rather mildly upon PDT in our samples, the impact on the P1 shunt should be relatively small. Indeed, when we analyse samples with different P1 widths, the shunt resistances do not differ systematically (see Sect. S.6). Additionally, we observed a similar effect of the PDT on the breakdown

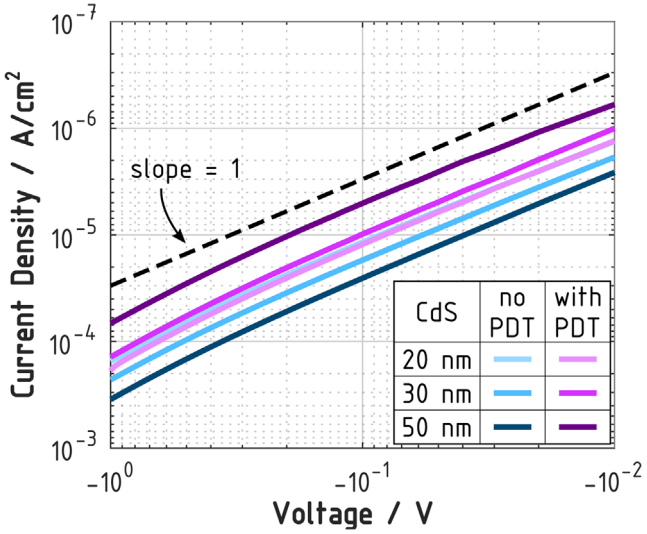

Fig. 5. Determining the nature of shunt leakage currents: Double-logarithmic representation of dark IV data averaged across 7–9 samples per cell type in the range from −1 V to 0 V. For comparison, the dashed black line indicates an ohmic behaviour with a slope of one.

characteristics in another batch of samples which we did not contact via the P lines. Therefore, it seems unlikely that the P1 scribe is a relevant shunt path in the investigated samples.

Another candidate for an ohmic shunt path are leakage currents via conduction along grain boundaries. Several studies indicate that these leakage currents are indeed reduced by an alkali-PDT: Cathodoluminescence imagings by Guthrey et al. [41] suggest that recombination at grain boundaries is reduced upon a KF-PDT. Similarly, Wuerz et al. [42] and Vilalta-Clemente et al. [43] show that Rb atoms accumulate at grain boundaries, and lifetime measurements by Ochoa et al. [44] indicate a reduced grain boundary recombination velocity after a RbF-PDT. Therefore, it seems likely that it is the effectiveness of shunt paths along grain boundaries that is reduced upon PDT in our samples due to reduced recombination and which in turn leads to the higher breakdown voltages observed for cells with PDT.

Revisiting the effect of buffer thickness on the reverse breakdown, alternatively or additionally to the tunneling mechanisms, the thickness of the buffer layer could also affect the quality of the layer in a way that a thinner layer leads to a higher number of localised shunts. This would increase the leakage current of the device and thus lower the breakdown voltage as suggested by Mack et al. [23] and Lee et al. [45]. In line with this hypothesis, the shunt resistance has been reported to increase with CdS thickness [46]. To test this relation in the current samples, we analyse the R_{sh} in Figure 4.

For the samples with PDT a clear trend towards higher R_{sh} with thicker buffer is visible, i.e. leakage currents seem to decrease with increasing thickness. This could indeed hint towards less shunts for thicker layers. An alternative interpretation may be a reduction of shunt leakage currents due to the increased series resistance of the buffer layer. For the samples without PDT, however, the trend is less clear (see also Sect. S.4). We assume that this is due to distortions caused by interface recombination (see above), which is expected to affect the shunt resistances. Therefore the results are less conclusive here. But in general a decrease in shunts upon buffer thickening could add to the tunneling mechanisms to explain the increase in breakdown voltage with buffer thickness. If indeed several different mechanisms are responsible for the breakdown behaviour, this could also explain the slightly different shapes of the reverse IV characteristics of the different cell types in Figure 1a by variations of the relative contributions of the mechanisms.

As a further interpretation of the *spectral* dependence of the reverse breakdown observed in Figure 1, shunt leakage currents could in principle be affected by the photoconductivity of the buffer [22] and window layers and thus lead to different breakdown voltages under red and white illumination. However, the shunt resistances extracted from the IV characteristics in these two cases do not differ substantially (see Sect. S.4). Only a slight tendency towards a lower shunt resistance under red than under white illumination is indicated, which cannot account for the large (opposite) differences observed in the breakdown voltages.

5 Conclusions

In this study we analysed the reverse IV characteristics of CIGS solar cells with and without a RbF-PDT and with different buffer layer thicknesses. We found that the breakdown voltage is significantly increased if (i) the absorber layer is treated with a RbF-PDT, (ii) the buffer layer thickness is increased, and (iii) the buffer layer is not photoexcited.

The results suggest that it is a combination of several mechanisms that play a role for the reverse breakdown: The buffer-thickness dependence gives strong evidence that the voltage drop in the buffer layer is essential for the reverse breakdown, probably by modulating tunneling currents over a conduction-band barrier and via defect levels in the band gap. Additionally, a recharging of defects or a pile-up of negative charges at the buffer/absorber interface seem to impact the reverse breakdown by influencing the electric field, as indicated by the significance of buffer photoexcitation.

Apart from this, also shunt leakage currents in the pre-breakdown voltage regime can affect the reverse breakdown by heating the material and thus facilitating breakdown. The investigations of the strong effect of PDT on the reverse breakdown indicated that the increase of breakdown voltage with PDT could be due a reduction of shunt leakage currents along grain boundaries by the heavy alkali.

On the other hand, the following mechanism could be ruled out to be responsible for the increased breakdown voltage upon PDT in the investigated samples: a change in potential fluctuations, a modified transport barrier, an improved homogeneity of the buffer layer thickness, and the increased bulk absorber doping density.

In light of the higher breakdown voltage, we would expect modules with PDT to be less tolerant against shading [47], because the dissipated electric power during operation under breakdown should be much higher than in

modules without PDT, which increases the probability of permanent damage. Therefore, an advanced understanding of the physics underlying the reverse breakdown in CIGS solar cells and their modification by an alkali-PDT seem highly relevant also from an industrial point of view. Whether or not the shading tolerance is indeed weakened upon PDT needs to be tested in separate experiments. Besides, further investigations of the reverse breakdown in material with different PDT processes will be necessary to evaluate whether the findings of this study show a general feature of an alkali PDT, and to what extent other effects of a PDT (e.g. a reduction of potential fluctuations) may possibly add further influences on the reverse breakdown behaviour.

We would like to thank Colleen Lattyak and David Nowak for help with the Raman experiments, Tash Motsi for the EQE measurements with light bias, and Matthias Maiberg and Roland Scheer for sharing their results of the transient V_{OC} measurements. The authors gratefully acknowledge funding by the German Ministry of Economic Affairs and Climate Action under grant "optiCIGS-II" (number 0324297F).

Author contribution statement

JN devised the study and did most of the measurements and data analysis. RS manufactured the sample variations. SJH devised the study, wrote the manuscript and did some measurements and data analysis.

Supplementary material

Supplementay material provided by the authors.

The Supplementary Material is available at https://www.epjpv.org/10.1051/epjpv/2022023/olm.

References

1. M. Richter et al., in *Proceedings of the 33rd EUPVSEC* (2017), pp. 1017-1019
2. E. Palmiotti et al., Sol. Energy **161**, 1 (2018)
3. K. Bakker et al., J. Mater. Res. **34**, 3977 (2019)
4. P. Szaniawski et al., Thin Solid Films **535**, 326 (2013)
5. R. Schäffler et al., Optimierte Qualitätsanalyse von CIGS-Modulen mittels bildgebender Messtechnik und Spektroskopie, Project report, Manz CIGS Technology GmbH, NICE Solar Energy GmbH, Bosch Solar CISTech GmbH, Forschungszentrum Jülich, Hochschule Ulm, Carl von Ossietzky Universität Oldenburg, Bayerisches Zentrum für Angewandte Energieforschung (2018)
6. X. Sun et al., in *42nd IEEE Photovoltaic Specialist Conference (PVSC)* (IEEE, 2015), pp. 1-6
7. P. Szaniawski et al., IEEE J. Photovolt. **7**, 1136 (2017)
8. H. Guthrey et al., Prog. Photovolt. Res. Appl. **27**, 812 (2019)
9. M. Richter et al., in *Proceedings of the 31st EUPVSEC* (2015), pp. 1069–1073
10. M. Richter et al., in *Proceedings of the 32nd EUPVSEC* (2016), pp. 1116–1119
11. F. Pianezzi et al., Phys. Chem. Chem. Phys. **16**, 8843 (2014)
12. S. Siebentritt et al., Adv. Energy Mater. **10**, 1903752 (2020)
13. M.H. Wolter et al., IEEE J. Photovolt. **8**, 1320 (2018)
14. A. Chirilă et al., Nat. Mater. **12**, 1107 (2013)
15. S. Puttnins et al., Sol. Energy Mater. Sol. Cells **120**, 506 (2014)
16. L. Mansfield, Manufacturing and Reliability Science for CIGS Photovoltaics, Technical report, National Renewable Energy Laboratory (2019)
17. F. Werner et al., Phys. Rev. Appl. **9**, 054047 (2018)
18. A. Zelenina et al., Appl. Phys. Lett. **111**, 213903 (2017)
19. L.M. Mansfield et al., in *IEEE 46th Photovoltaic Specialist Conference (PVSC)* (2019), pp. 3201–3205
20. S. Puttnins et al., in *Proceedings of the 26th EUPVSEC* (2014), pp. 2432–2434
21. T.J. Nagle, Ph.D. thesis, Colorado State University (2007)
22. D. Braunger et al., Sol. Energy Mater. Sol. Cells **40**, 97 (1996)
23. P. Mack et al., in *Proceedings of the 23rd EUPVSEC* (2008), pp. 2156–2159
24. P. Mack et al., in *Proceedings of the 24th EUPVSEC* (2009), pp. 2439–2442
25. F. Obereigner et al., J. Appl. Phys. **117**, 055704 (2015)
26. M.S. Lyam et al., J. Appl. Phys. **129**, 205703 (2021)
27. Y.-H. Chang et al., Adv. Funct. Mater. **31**, 2103663 (2021)
28. M. Troviano et al., in *Proceedings of the 24th EUPVSEC* (2009), pp. 2933–2937
29. T. Kodalle et al., Sol. RRL **2**, 1800156 (2018)
30. F. Werner et al., Thin Solid Films **633**, 222 (2017)
31. M. Rusu et al., ACS Appl. Mater. Interfaces **13**, 7745 (2021)
32. N. Taguchi et al., Appl. Phys. Lett. **113**, 113903 (2018)
33. E. Handick et al., ACS Appl. Mater. Interfaces **7**, 27414 (2015)
34. S. Cheng et al., ACS Appl. Energy Mater. **4**, 3279 (2021)
35. F. Werner et al., Prog. Photovolt. Res. Appl. **26**, 911 (2018)
36. G. Sozzi et al., in *44th IEEE Photovoltaic Specialist Conference (PVSC)* (2017), pp. 2205–2208
37. B.L. Williams et al., Prog. Photovolt. Res. Appl. **23**, 1516 (2015)
38. S. Dongaonkar et al., J. Appl. Phys. **108**, 124509 (2010)
39. C. Schubbert et al., Sol. Energy Mater. Sol. Cells **157**, 146 (2016)
40. A. Virtuani et al., Thin Solid Films **451–452**, 160 (2004)
41. H. Guthrey et al., IEEE J. Photovolt. **8**, 1833 (2018)
42. R. Wuerz et al., J. Appl. Phys. **124**, 165305 (2018)
43. A. Vilalta-Clemente et al., Appl. Phys. Lett. **112**, 103105 (2018)
44. M. Ochoa et al., Adv. Energy Mater. **12**, 2102800 (2022)
45. J.E. Lee et al., Prog. Photovolt. Res. Appl. **24**, 1035 (2016)
46. A. Virtuani et al., Thin Solid Films **431**, 443 (2003)
47. T.J. Silverman et al., IEEE J. Photovolt. **5**, 1742 (2015)
48. P. Schöppe et al., ACS Appl. Mater. Interfaces **10**, 40592 (2018)

Cite this article as: Janet Neerken, Raymund Schäffler, Stephan J. Heise, Exploring reverse-bias characteristics of CIGS solar cells: impact of alkali-post-deposition treatment and CdS buffer layer, EPJ Photovoltaics **13**, 26 (2022)